Supporting Information

The Soybean Lipoxygenase-Substrate Complex: Correlation Between Properties of Tunneling-Ready States and ENDOR-Detected Structures of Ground States

Adam R. Offenbacher,[1,2*] Ajay Sharma,[3] Peter E. Doan,[3] Judith P. Klinman,[2,4*] Brian M. Hoffman[3,5*].

[1]Department of Chemistry, East Carolina University, Greenville, North Carolina 27858; [2]Department of Chemistry and California Institute for Quantitative Biosciences (QB3), University of California, Berkeley, California 94720; [3]Department of Chemistry, Northwestern University, Evanston, Illinois 60208; [4]Department of Molecular and Cell Biology, University of California, Berkeley, California 94720; and [5]Department of Molecular Biosciences, Northwestern University, Evanston, Illinois 60208.

* To whom correspondence should be addressed:

offenbachera17@ecu.edu;

klinman@berkeley.edu;

bmh@northwestern.edu.

EPR/ENDOR Simulations: Simulations in our previous publication employed the program, EasySpin[1], which has provisions for calculating spectra obtained by the full suite of paramagnetic resonance techniques. However, simulation of low-temperature EPR and ENDOR spectra of the zero-field split S = 5/2 Mn^{2+} ion is particularly difficult, with the major issues that complicate a description being differential nutation of the individual EPR manifolds and differential phase memory for the different manifolds. We observed that in part at least as a result of these issues, EasySpin gave distorted ^{13}C ENDOR intensity envelopes. As a result, when that program was used to decompose the ^{13}C ENDOR spectra into *a* and *b* contributions it led to overestimates of the *a* conformer occupancy, as noted in the main text. Because of this, a purpose-written (Latin: *ad hoc*) Mn^{2+} ENDOR simulation program was written in Mathcad Prime.® We chose to use a Monte Carlo method to generate individual orientations. It uses great circles on the unit sphere that are random generated, rather than using a deterministic approach that defines previous ENDOR simulation protocols. We start with the values of the D tensor (D_x,D_y,D_z) and a D-strain tensor (σ_x,σ_y,σ_z). All calculations assume that the $|4D_z| << g\beta_e B$ (~35 GHz) so that a simple 1st order approximation is adequate for this system. (S, m_s good quantum numbers).

The ENDOR simulations give a rigorously proper treatment of Mims 'holes', which is a non-trivial issue in this case, when multiple EPR manifolds overlap. An isotropic ENDOR lineshape is applied after calculation of the intensity envelopes that include the Mims suppression effects. Because of the intrinsic difficulty in simulating the response from a Mn^{2+} at low temperatures, as mentioned above, these simulations still by no means perfect as seen below in **Fig S7**. However, the simulations not only give the hyperfine interaction parameters with precision, but now also reproduce the ENDOR envelopes with sufficient fidelity to yield robust values for the variation in conformer occupancies when used on the suite of SLO mutants to decompose their ^{13}C ENDOR spectra into contributions from *a* and *b* conformers.

These new simulations are applied in two principal ways. *(1)* They are used to obtain the dipolar interaction tensors, ***T***, that describe the hyperfine interactions between Mn^{2+} and LA labeled with ^{13}C at specific sites; see **Figure S1**. For this purpose, the two programs give comparable results, and thus comparable Mn-^{13}C distances. *(2)* The new simulations are used to decompose the $^{13}C11$ spectra collected at the low-field edge of the EPR envelope into contributions from *a* and *b* conformers, as illustrated for Ile553 in **Figure 3A**, and for all 553X in **Figure S7**. These decompositions robustly quantify the variation with mutation in the fractional *a* occupancy, f_a, which is tabulated in **Table S1**.

Optimization of ^{13}C Mims ENDOR response: In comparison with our previous work (Horitani et. al. *J. Am. Chem. Soc.* **2017**, *139*, 1984-1997), with the availability of the enhanced MW power, we could optimize τ in the Mims ENDOR pulse sequence to maximize the S/N ratio of the ^{13}C ENDOR response. The $^{13}C11$ hyperfine coupling of the substrate linoleic acid (LA) is dominated by through-space dipolar coupling (T) with negligible contribution from isotropic hyperfine coupling (A_{iso}). The ENDOR response in a Mims sequence is given as $I \propto 2\sin^2(\pi A\tau)$, where A is the hyperfine coupling, and τ is the time difference between first two MW pulses. For very small values of A, $I \propto \tau^2$. Although the response thus increases with τ, the echo intensity fall with increasing τ. In our current studies all ^{13}C Mims ENDOR is recorded at the value τ = 1500 ns which optimized the S/N of the ENDOR signal, increasing it bay ~ 9 times better than for the signal recorded at τ = 500ns which was employed in our previous publication (Horitani et. al) (Figure S3)

*Decomposition of ^{13}C11 Mims ENDOR spectra (**figure S7**):* It is important to stress that we are reporting the robustly measured fractional populations of conformers with a properly bound (aligned) substrate: the enzymatically active *a* conformer and the *b* non-reactive conformer. Within the resolution of these measurements it is adequate to treat each of these populations as having a smooth distribution of the ^{13}C11-Mn^{2} distances whose breadth is inferred from the linewidth (**eq 3**), and as illustrated in **Figs 3A** and especially **S7**.

Figure S7 in particular highlights the importance of properly incorporating the effects of Mims 'holes' (mentioned above). Every spectrum in this figure shows a minimum at the Larmor frequency ν(13C) that is the Mims hole ($A\tau = 0$). Without this hole, the response in this region would be flat and visual inspection would support the decomposition into two conformers. Without a recognition of the origin of this minimum, it instead gives the illusion of a distinct signal at very small offset, which could be assigned to a distinct *b* sub-population.

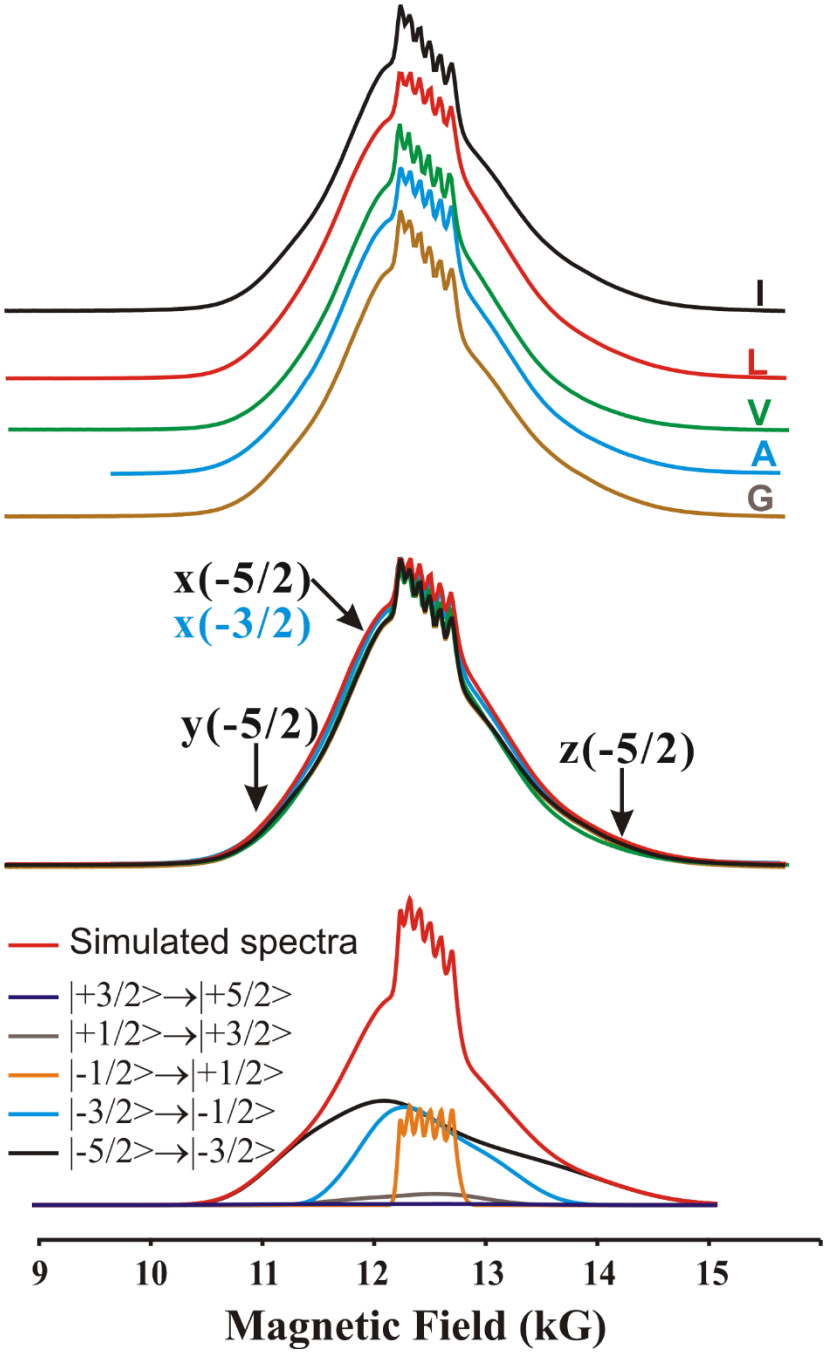

Figure S1. 35 GHz, 2K, ESE-EPR spectra for WT and four mutants of SLO-LA complex (top) and the overlay (middle). The magnetic fields indicated by arrows represent the "crystal field" like position (when the magnetic field is along the three principal axes of the ZFS (x, y, z). Partitioning of the EPR spectra of WT into contributions from the five electron spin transitions of Mn^{2+} (bottom). EPR simulation parameters: zero field parameters D(X, Y, Z) Dx = -660 MHz, Dy = -220 MHz, Dz = 880 MHz; D strain parameters (25, 25, 50) MHz. EPR simulations were carried out using Easyspin. *Conditions:* microwave frequency ~ 34.8 GHz, MW pulse length ($\pi/2$) = 40 ns, τ = 400 ns, repetition rate =100 Hz.

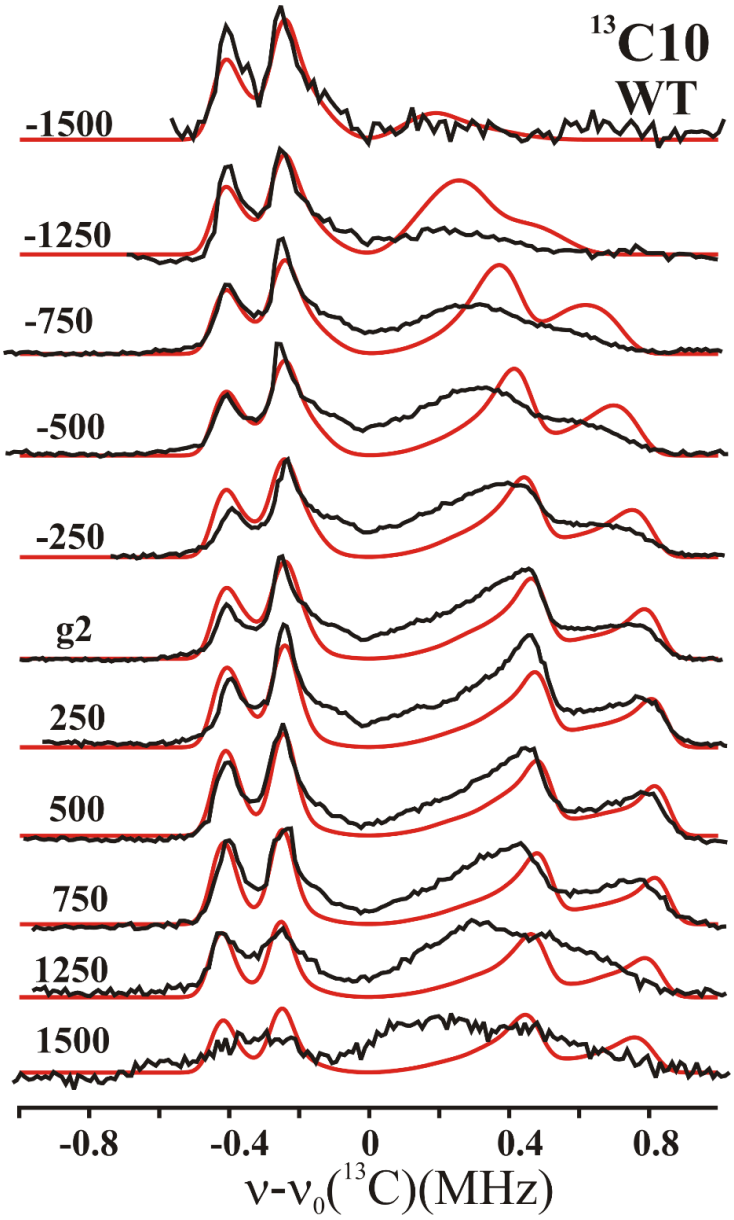

Figure S2. 35 GHz 2D field-frequency pattern of ^{13}C Mims ENDOR spectra for Mn-SLO WT with ^{13}C10-LA collected at different magnetic fields across the EPR envelope (black). g2 corresponds to g = 2 (magnetic field, 12.5kG), the center of the EPR envelope; spectrum shown in Fig. S1) The ENDOR spectra are recorded at magnetic fields offset from g = 2 as indicated. Simulation (red) of the ENDOR spectra using the new algorithm described in SI above. *Simulation parameters:* zero field parameters D(X, Y, Z) Dx = -660 MHz, Dy = -220 MHz, Dz = 880 MHz; D strain parameters (25, 25, 50) MHz, dipolar parameter *T* = 0.17 MHz, (ϕ ~ 90, θ ~ 50), W = 50 KHz, T = 2 K. In the coordinate system used in this simulation, ϕ is defined as the rotation about the principal ZFS (z) axis away from the x axis, so ϕ = 90 corresponds to the z-y plane.
Mims ENDOR Conditions: microwave frequency ~ 34.8 GHz, MW pulse length (π/2) = 50 ns, τ = 1500 ns, repetition rate =100 Hz, and T = 2 K.

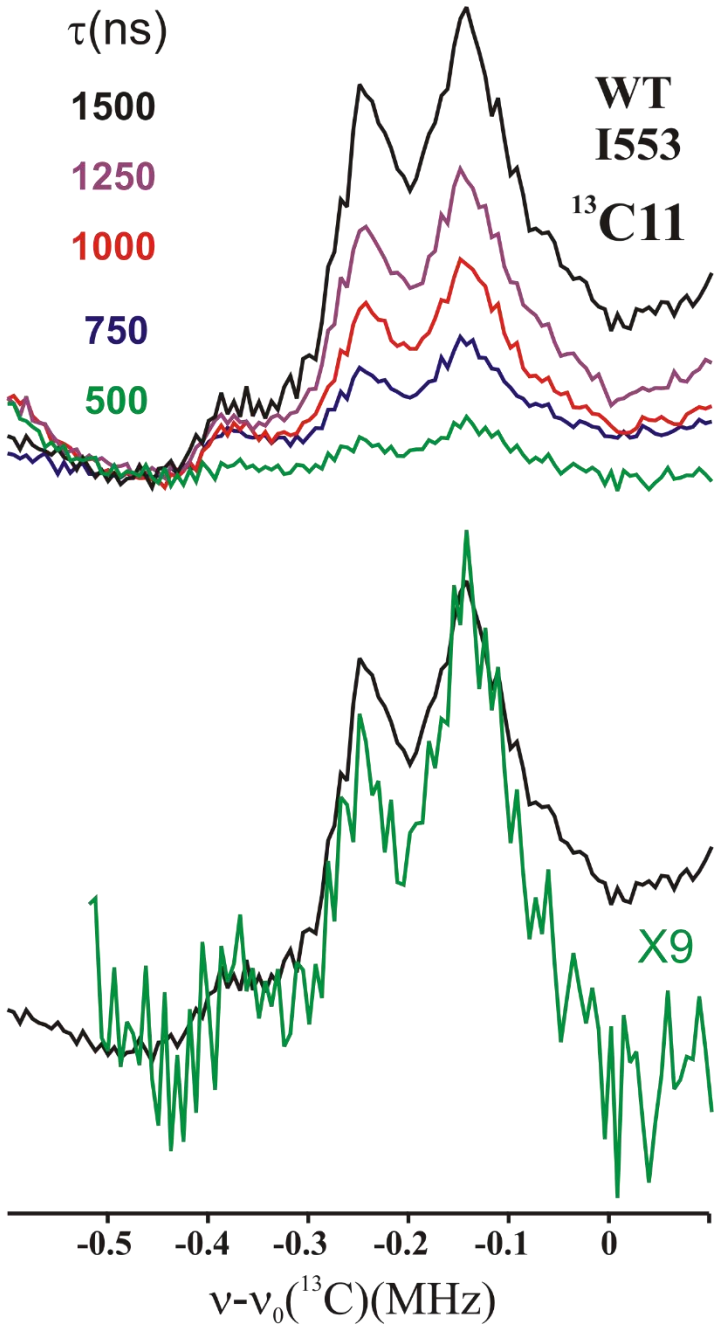

Figure S3. ^{13}C11 Mims ENDOR spectra for Mn-SLO WT with ^{13}C11-LA recorded at different τ values (top). The S/N ratio increases by 9 times when τ is increases from 500 to 1500 ns (bottom). Experimental conditions as in Figure S2, Magnetic field H = 11kG.

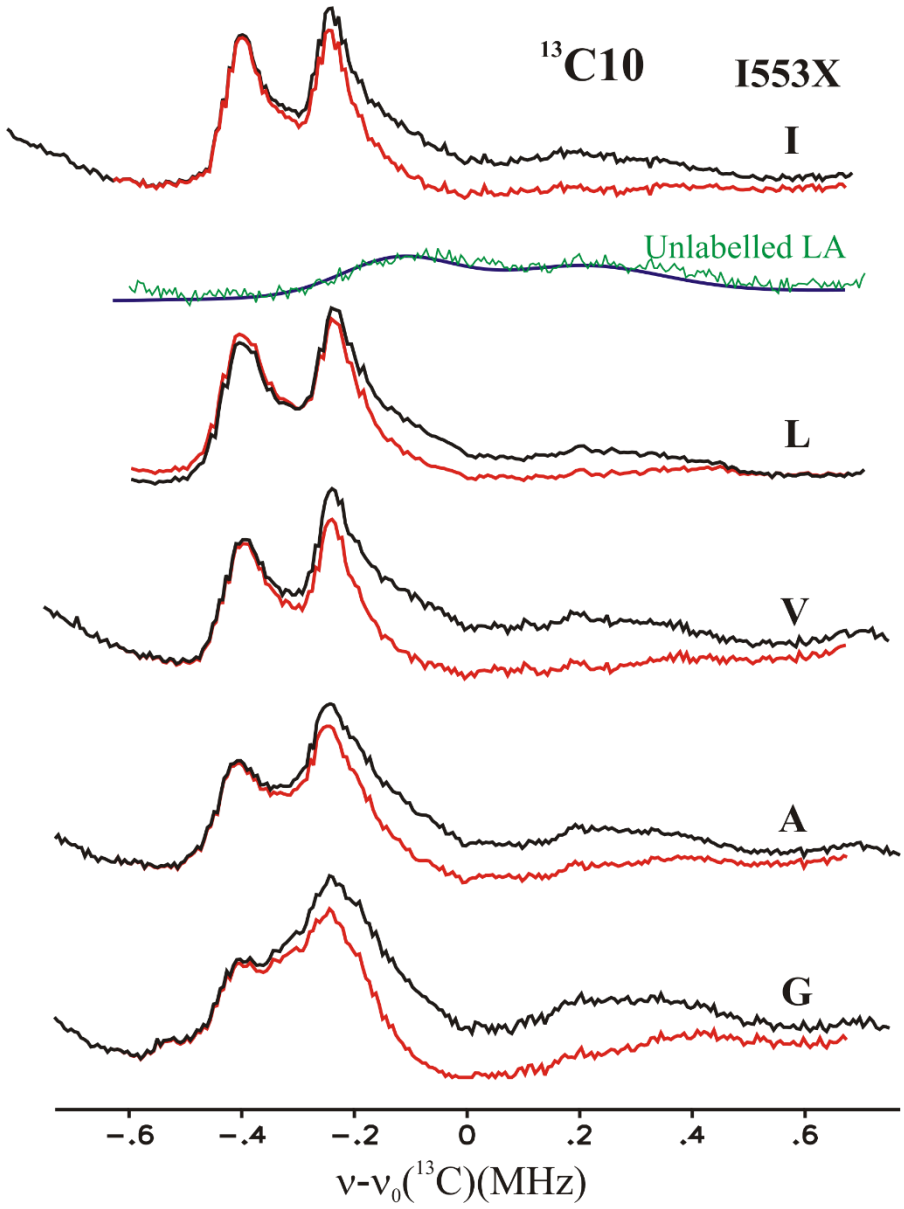

Figure S4. Background-subtracted ^{13}C10 Mims ENDOR spectra for I553X series with ^{13}C10-LA (red). The signals from the selectively ^{13}C labelled substrate (black) were isolated from those of natural-abundance ^{13}C by subtraction of a fit (blue) to a corresponding spectrum with the natural-abundance substrate (green). The ENDOR response from the natural abundance ^{13}C is fitted to two Gaussian and the fitted spectrum is used for all background subtraction. Experimental conditions as in Figure S3.

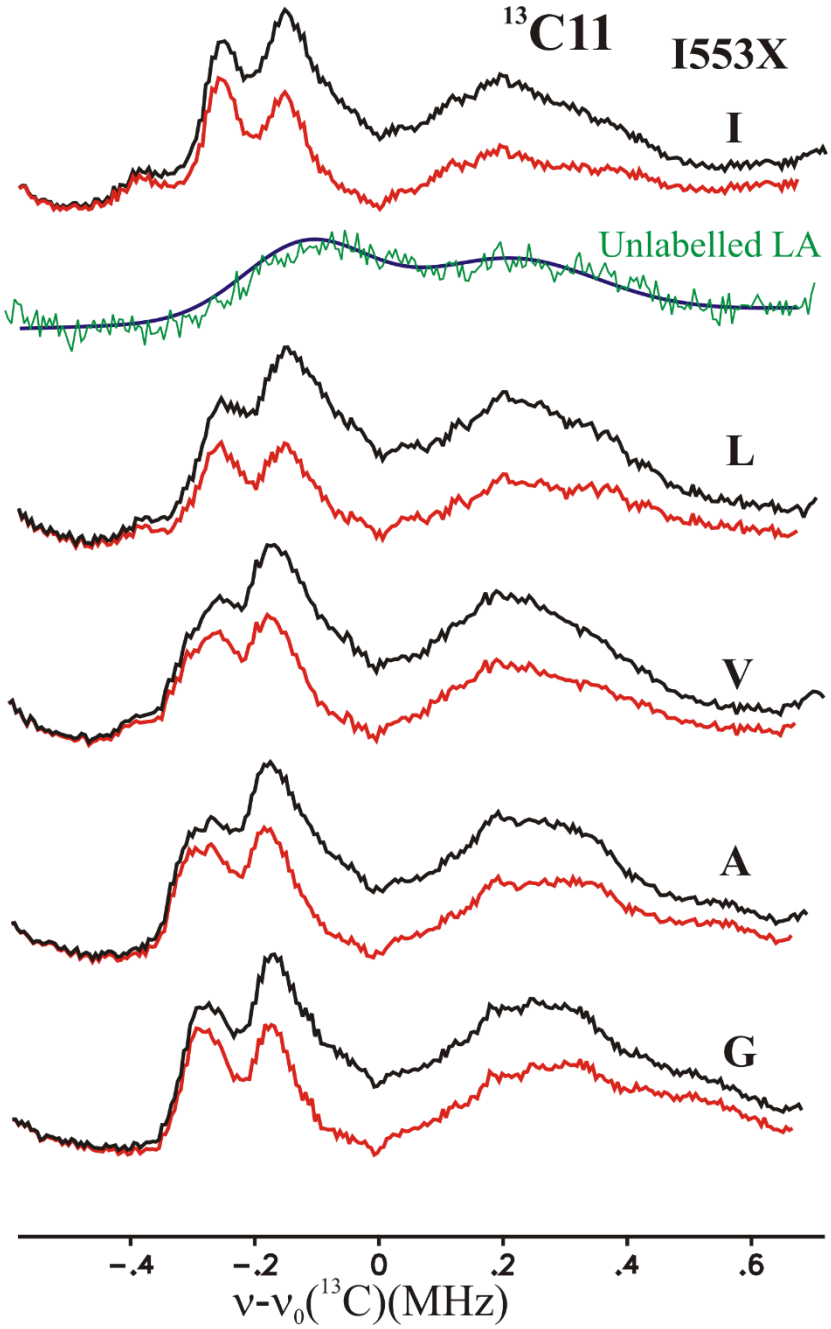

Figure S5. Background subtracted ^{13}C11 Mims ENDOR spectra for I553X series with ^{13}C11-LA (red). The signals from the selectively ^{13}C labelled substrate (black) were isolated from those of natural-abundance ^{13}C by subtraction of a corresponding spectrum with the natural-abundance substrate (green). The ENDOR response from the natural abundance ^{13}C is fitted to two Gaussian and the fitted spectrum is used for all background subtraction Experimental conditions as in Figure S3.

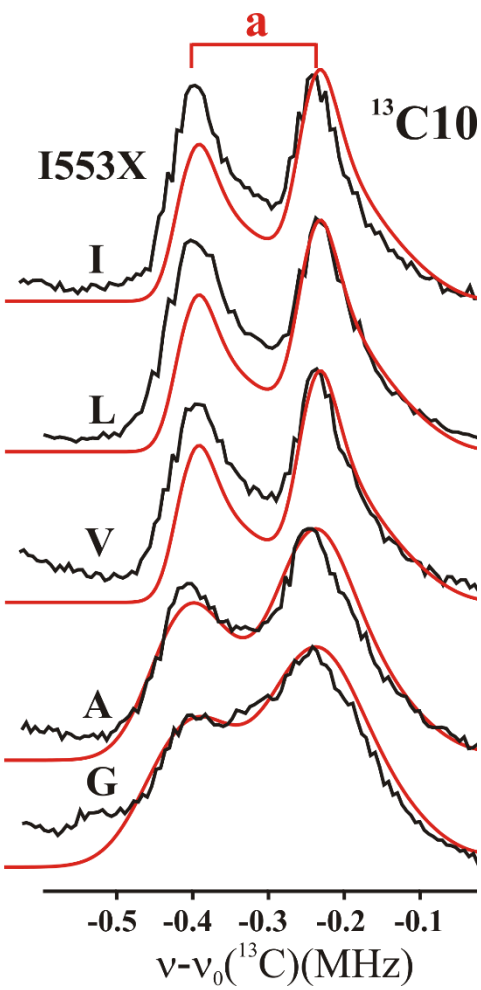

Figure S6. ^{13}C10 Mims ENDOR spectra of I553X series; experimental (black) simulation (red). Simulation parameters are tabulated in **Table S3**. The position of C10 of substrate LA from Mn remains the same, and in the two conformers *a, b*, unchanged by the mutations. *Experimental conditions:* as in Figure S3

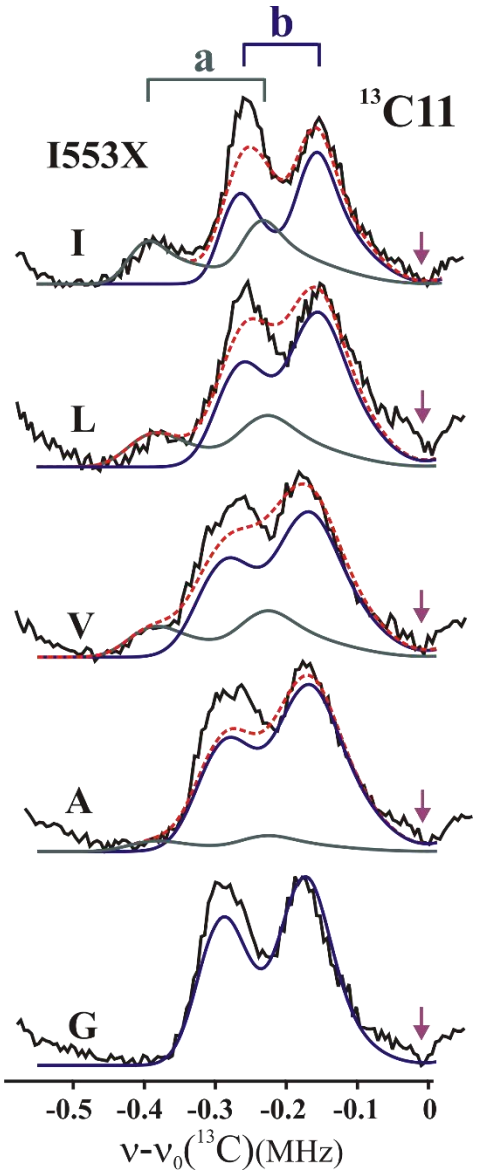

Figure S7. ^{13}C11 Mims ENDOR spectra of I553X series. The arrow at the Larmor frequency identifies the Mims 'hole' at $\nu_0(^{13}C)$ ($A\tau = 0$) as explained above in SI text. The simulations of the responses for the two LA conformer populations, '*a*' (green), '*b*' (blue) and their sum (red) are shown. The occupancy of *a* and *b* conformers is estimated by fitting a a summation of the simulations to the experimental spectra with f_a as the fit parameter. Given the limitations in the simulations, noted in the text above, the fit protocol involves fixing the contribution from the *a* manifold by matching the intensity of the peak at ~0.4 MHz of *a* only conformer, and then adding sufficient *b* spectrum to match the peak at ~0.17 MHz, arising only from *b* conformer. This process avoids the complications that arise with the peak 'in the middle' at ~0.3 MHz, which has significant overlapped contributions from both *a* and *b* conformers and is not well reproduced.The simulation parameters are tabulated in **Table S1**. The critical parameter, the percentage occupancy of active *a* conformer, denoted f_a, is tabulated in **Table S2**. *Experimental conditions:* as in **Figure S3.**

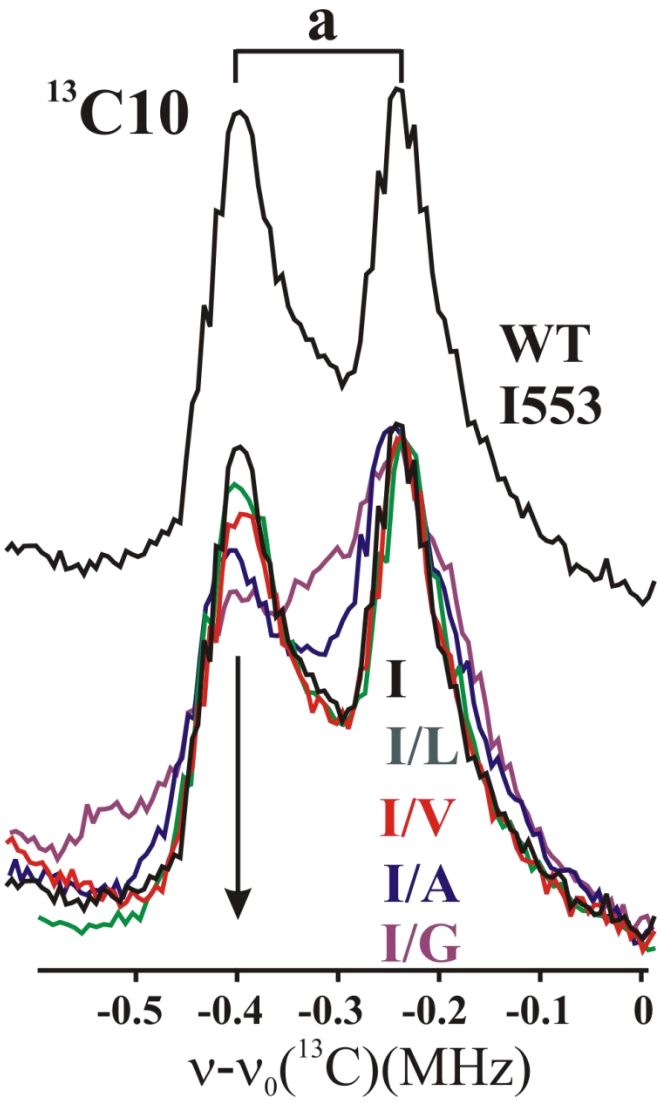

Figure S8. ^{13}C Mims ENDOR spectra of C10 of the enzyme-substrate complex of I553X series. *Top*, spectrum of WT enzyme. *Bottom*, overlay normalized to amplitude of the ~ -0.2 MHz peak to highlight variations caused by mutations. For example, only X = A shows a very slight increase in offset; linewidth increases very slightly for X = V and more for A, but significantly for X = G, as discussed in text. *Conditions:* as in **Figure S1.**

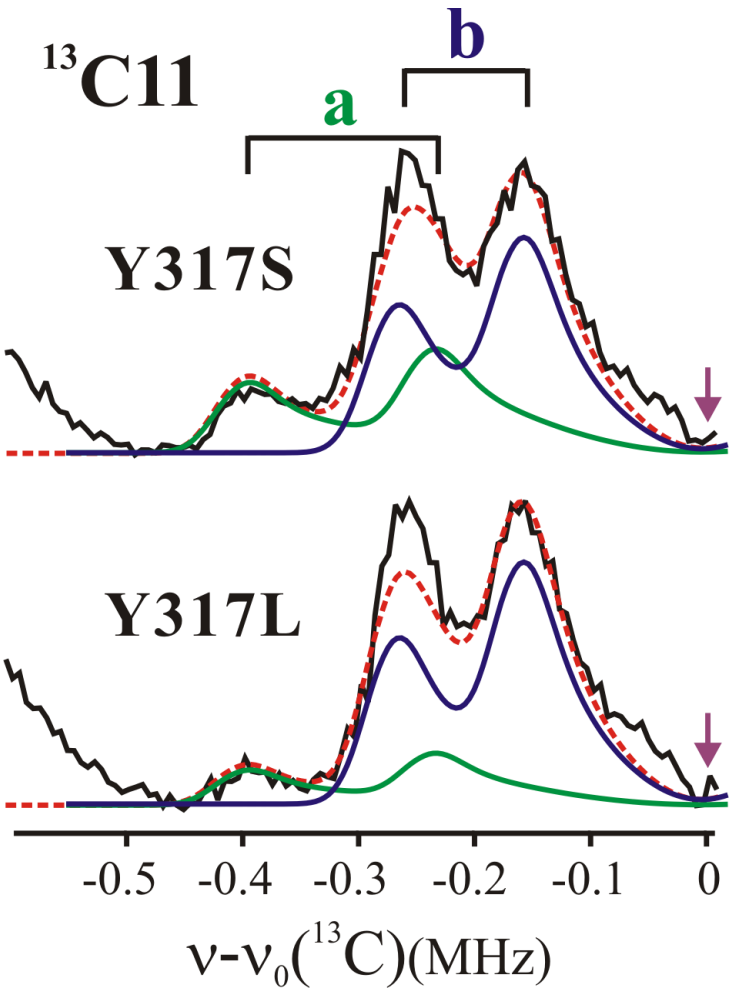

Figure S9. The ^{13}C11 Mims ENDOR spectra of Tyr317X series from **Figure 5B**. The simulated decompositions of the spectrum into contributions from the two conformers "*a (green)* and *b* (blue) are also (dashed red). In keeping with **Fig S7**, the arrows identify the Mims 'hole' at $\nu_0(^{13}C)$. *Simulation parameters* listed in **Table S1**. *Experimental conditions:* as in **Figure S1.**

Table S1. ENDOR simulation parameters used in decomposition of ^{13}C11 ENDOR spectra of active mutants; I553X (X = Leu, Val, Ala, Gly) and loop mutants Y317L, Y317S shown in **Figure S7**; occupancies in **Table S2**.

SLO variant	Conformer	*r* (Å)[b]	*t(r)* (MHz)	(θ, ϕ) deg	*δr* (Å)[c]	*W* (kHz)
Ile553[a] (WT)	*a*	4.90	0.17	(50, 90)		50
	b	5.65	0.11	(60, 90)		50
I/Leu	*a*	4.90	0.17	(50, 90)	0.08	70
	b	5.65	0.11	(60, 90)	0.14	70
I/Val	*a*	4.90	0.17	(50, 90)	0.09	70
	b	5.49	0.12	(60, 90)	0.18	80
I/Ala	*a*	4.90	0.17	(50, 90)	0.08	70
	b	5.49	0.12	(60, 90)	0.18	80
I/Gly						
	b	5.49	0.12	(60, 90)	0.12	70
Loop mutants						
Y317L	*a*	4.90	0.17	(50, 90)	~0	50
	b	5.65	0.11	(60, 90)	~0	50
Y317S	*a*	4.90	0.17	(50, 90)	~0	50
	b	5.65	0.11	(60, 90)	~0	50

[a]As noted above, the decompositions yield robust ^{13}C11 conformer occupancies.
[b]Mn-C distance *r* is calculated using Eq. 1.
[c]*δr*, distribution in distances around average *r* are calculated using Eq. 3. Within the limits of resolution, the ENDOR offset, *δv*, for the *a* conformer, and thus *t(r)* and the calculated Mn-^{13}C11 distance, *r*, does not vary as 553 varies, but in *b*, the offset (and *t(r)*) slightly increases for the smaller residues.

Table S2. ***Upper:*** Comparison between ENDOR *a* conformer occupancy percentage (f_a) sidechain volume, differential enthalpic barrier for D and H transfer (ΔE_a), and calculated[2] equilibrium distance (R_0) and DAD sampling frequency (ω) for SLO I553X variants. ***Lower:*** Occupancy percentage (f_a) and ΔE_a for Loop mutants. The occupancy of the *a* conformer is estimated by a summation of the simulation to fit the experimental spectrum as described in the legend to **Fig S7**.

SLO variant	f_a(%)[a]	Sidechain volume (A^3)[b]	ΔE_a (kcal/mol)	R_0, Å [c]	ω, cm^{-1} [c]
Ile553 (WT)	20 (2)	167	0.9 (0.2)[d]	2.85	320
553Leu	15 (2.5)	167	3.4 (0.6)[e]	3.07	243
553Val	13 (2)	140	2.6 (0.5)[e]	2.97	271
553Ala	5 (2)	89	4.0 (0.3)[d]	3.04	252
553Gly	0 (3)[f]	60	5.3 (0.7)[e]	3.32	218
Loop mutants					
Y317L	15(2)		2.3 (0.2)		
Y317S	20(2)		1.2 (0.2)		

[a]Uncertainty in f_a is $\pm(\delta f_a)$, except as noted.
[b]From ref: [3]
[c]The equilibrium DAD, R_0, which represents the distance computed prior to the onset of distance sampling, and the DAD frequency, ω, were determined from the analytical rate expression using quadratic terms and mass of M = 14 amu, as described (including parameters) in reference 2.
[d]From ref [4]
[e]From ref [5]
[f]Uncertainty is $+(\delta f_a)$

Table S3. Simulation Parameters for I553X ^{13}C10 ENDOR spectra shown in **Figure S3**

SLO variant	*r* (Å)	*t(r)* (MHz)	(θ, ϕ) deg	δr (Å)	*W* (kHz)
Ile553 (WT)	4.9	0.17	(50,90)		50
553Leu	4.9	0.17	(50,90)	~0	50
553Val	4.9	0.17	(50,90)	~0	50
553Ala	4.9	0.17	(50,90)	0.19	100
553Gly	4.9	0.17	(50,90)	0.27	120

Table S4. Kinetic parameters for WT SLO and mutants[a]

SLO variant	k_{cat}, s^{-1}	E_a, kcal/mol	$^{D}k_{cat}$	ΔE_a, kcal/mol
WT[b]	297 (10)	2.1 (0.2)	81 (5)	0.9 (0.2)
	Active site mutants			
I553L[c]	273 (10)	0.4 (0.7)	81 (3)	3.4 (0.6)
I553V[c]	91 (5)	2.4 (0.5)	77 (6)	2.6 (0.5)
I553A[b]	280 (10)	1.9 (0.2)	93 (4)	4.0 (0.3)
I553G[c]	58 (4)	0.03 (0.04)	178 (16)	5.3 (0.7)
	Loop mutants[d]			
Y317L	368 (8)	1.0 (0.1)	67 (2)	2.3 (0.2)
Y317S	330 (8)	2.3 (0.2)	64 (2)	1.2 (0.2)

[a]Conditions are 0.1 M borate, pH 9.0. k_{cat} values are reported at 30˚C.
[b]From ref [4]
[c]From ref [5]
[d]k_{cat} values are higher; attributed to difference in purification procedures. $^{D}k_{cat}$ values are consistently decreased for this new purification procedure. For this revised procedure, WT k_{cat} $^{D}k_{cat}$ values were determined as 359 (7) s^{-1} and 57 (2), respectively. All other parameters are directly comparable. From ref [6]

References

[1] Stoll, S., and Schweiger, A. (2006) Easyspin, a comprehensive software package for spectral simulation and analysis in EPR, *J. Magn. Reson. 178*, 42-55.

[2] Hu, S., Soudachkov, A. V., Hammes-Schiffer, S., and Klinman, J. P. (2017) Enhanced rigidifcation within a double mutant of soybean lipoxygenase provides experimental support for vibronically nonadiabatic proton-coupled electron transfer models, *ACS Catal. 7*, 3569-3574.

[3] Zamyatnin, A. A. (1972) Protein volume in solution, *Prog. Biophys. Mol. Biol. 24*, 107-123.

[4] Knapp, M. J., Rickert, K. W., and Klinman, J. K. (2002) Temperature-dependent isotope effects in soybean lipoxygenase-1: correlating hydrogen tunneling with protein dynamics, *J. Am. Chem. Soc. 124*, 3865-3874.

[5] Meyer, M. P., Tomchick, D. R., and Klinman, J. K. (2008) Enzyme structure and dynamics affect hydrogen tunneling: the impact of a remote side chain (I553) in soybean lipoxygenase-1, *Proc. Natl. Acad. Sci. U. S. A. 105*, 1146-1151.

[6] Offenbacher, A. R., Hu, S., Poss, E. M., Carr, C. A., Scouras, A. D., Prigozhin, D. M., Iavarone, A. T., Palla, A., Alber, T., Fraser, J. S., and Klinman, J. P. (2017) Hydrogen-deuterium exchange of lipoxygenase uncovers a relationship between the distal, solvent exposed protein motions and the thermal activation barrier for catalytic proton-coupled electron tunneling, *ACS Cent. Sci 3*, 570-579.